Lamina Cribrosa Insertions Into the Sclera Are Sparser, Narrower, and More Slanted in the Anterior Lamina

Fengting Ji,[1,2] Mohammad R. Islam,[1,3] Bingrui Wang,[1] Yi Hua,[1,4] and Ian A. Sigal[1,2]

[1]Department of Ophthalmology, University of Pittsburgh, Pittsburgh, Pennsylvania, United States
[2]Department of Bioengineering, University of Pittsburgh, Pittsburgh, Pennsylvania, United States
[3]Department of Mechanical Engineering, University of Texas Rio Grande Valley, Edinburg, Texas, United States
[4]Department of Biomedical Engineering, University of Mississippi, University, Mississippi, United States

Correspondence: Ian A. Sigal, Laboratory of Ocular Biomechanics, Department of Ophthalmology, University of Pittsburgh, 1622 Locust St., Rm. 7.382, Pittsburgh, PA 15219, USA;
ian@ocularbiomechanics.com.

Received: December 12, 2023
Accepted: April 3, 2024
Published: April 22, 2024

Citation: Ji F, Islam MR, Wang B, Hua Y, Sigal IA. Lamina cribrosa insertions into the sclera are sparser, narrower, and more slanted in the anterior lamina. *Invest Ophthalmol Vis Sci.* 2024;65(4):35. https://doi.org/10.1167/iovs.65.4.35

Purpose. The lamina cribrosa (LC) depends on the sclera for support. The support must be provided through the LC insertions. Although a continuous insertion over the whole LC periphery is often assumed, LC insertions are actually discrete locations where LC collagenous beams meet the sclera. We hypothesized that LC insertions vary in number, size, and shape by quadrant and depth.

Methods. Coronal cryosections through the full LCs from six healthy monkey eyes were imaged using instant polarized light microscopy. The images were registered into a stack, on which we manually marked LC insertion outlines, nothing their position in-depth and quadrant (inferior, superior, nasal, or temporal). From the marks, we determined the insertion number, width, angle to the canal wall (90 degrees = perpendicular), and insertion ratio (fraction of LC periphery represented by insertions). Using linear mixed effect models, we determined if the insertion characteristics were associated with depth or quadrant.

Results. Insertions in the anterior LC were sparser, narrower, and more slanted than those in deeper LC (P values < 0.001). There were more insertions spanning a larger ratio of the canal wall in the middle LC than in the anterior and posterior (P values < 0.001). In the nasal quadrant, the insertion angles were significantly smaller ($P < 0.001$).

Conclusions. LC insertions vary substantially and significantly over the canal. The sparser, narrower, and more slanted insertions of the anterior-most LC may not provide the robust support afforded by insertions of the middle and posterior LC. These variations may contribute to the progressive deepening of the LC and regional susceptibility to glaucoma.

Keywords: lamina cribrosa (LC), insertion, collagen, sclera, glaucoma

The retinal ganglion cell axons that transmit visual information from the retina to the brain pass through the lamina cribrosa (LC), a collagenous region within the optic nerve head (ONH) where they exit the globe.[1,2] The mechanical support provided by the LC collagen is believed to be essential for the fragile neural tissues within the LC to withstand the forces caused by intraocular pressure (IOP), gaze changes, and other mechanical challenges that could otherwise lead to neuropathy and vision loss.[3–9] The ability of the LC to protect the neural tissues is intrinsically dependent on the support that the LC receives from the much stronger surrounding peripapillary sclera.[7,8,10,11] Where the LC and the sclera meet, often referred to as the LC insertion, serves thus the crucial role of connecting the two tissues and transmitting forces between them. The LC insertions therefore play a critical role in influencing the biomechanical robustness of the LC, including the sensitivity to elevated IOP and with this the susceptibility to glaucomatous neural tissue damage. In the classic description, the LC insertion is the boundary between the LC and sclera, taking the form of a line in 2D views, such as histological sections, or a surface in 3D models (Fig. 1). This LC insertion is often characterized by the location of its most anterior and posterior points, the anterior LC insertion and posterior LC insertion, respectively.[12]

Largely due to the important role of the LC in glaucoma, several studies have been conducted to characterize LC insertions and their structural changes during aging or the development of glaucoma.[13–19] The studies revealed, for instance, that the location of the anterior and posterior LC insertions change with glaucoma. More specifically, using histomorphometry of tissues from an experimental monkey model of glaucoma, the authors found that both anterior and posterior LC insertions become more posterior early in the pathology.[12] The observation was later confirmed in humans using optical coherence tomography (OCT).[18] Other studies have described other simple morphological aspects of the insertions, such as length and depth or their variations over quadrants.[13,18,20–23] This information has been used in biomechanical analyses to understand their role in sensitivity to IOP and glaucomatous neuropathy.[4,24–26] Despite the valuable information gained, a major limitation of the studies described above is that they have been largely based on a simplistic description of the LC insertion as a

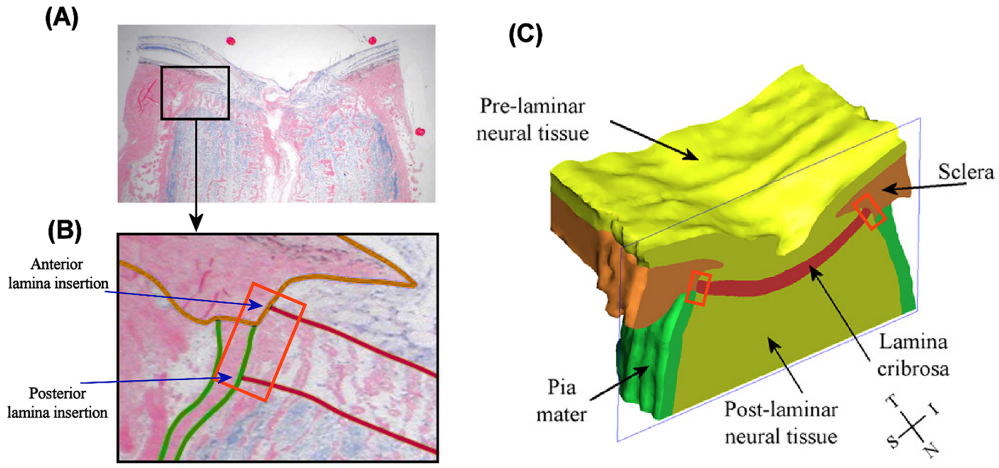

Figure 1. (**A**) Bright field images of a section of human ONH labeled with *picrisirius red* for collagen and *solochrome cyanin* for neural tissues. (**B**) Close up of the canal periphery in **A**. *Orange lines* show the outline of the sclera, the *green* outlines the internal and external pia mater, and the *red* lines show the anterior and posterior boundaries of the LC. The conventional characterization of the LC considers the insertion to be continuous from the anterior lamina insertion to the posterior lamina insertion. **A** and **B** adapted from Ref. 13 images originally presented in Ref. 20. (**C**) The simplest approach to define the LC insertion has been applied in the reconstruction of mechanical models of the ONH, where the assumption of insertion continuity is extended in 3D surface between the LC and canal edge. The image shows a 3D specimen specific model adapted from Ref. 27. In both **B** and **C**, the LC insertion regions are highlighted using *red boxes*.

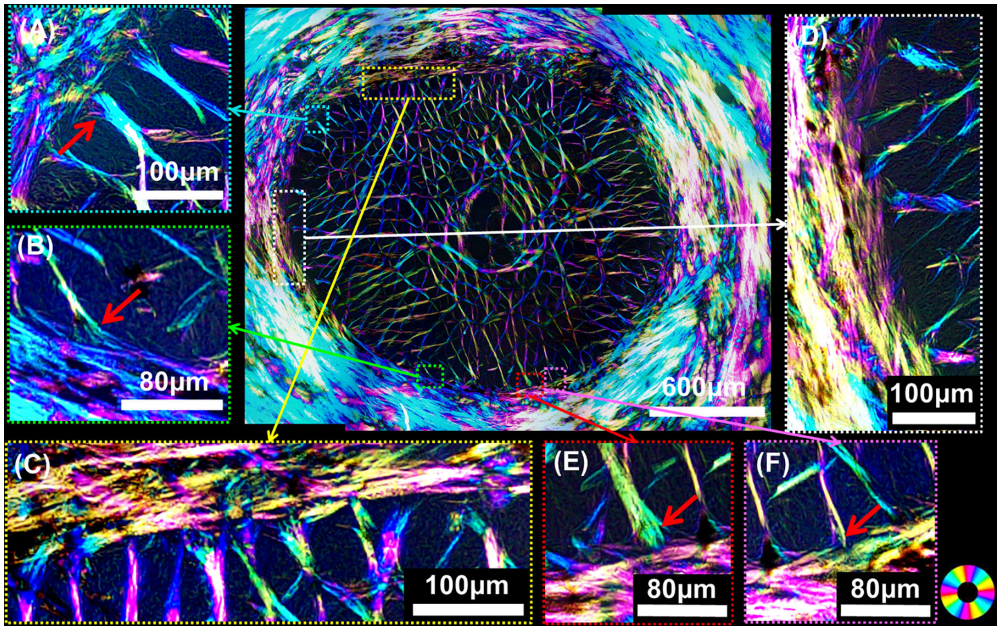

Figure 2. Example IPOL image of a monkey ONH coronal cryosection, showing the variations of LC insertions. The image was acquired with an objective with higher resolution (0.66 μm/pixel) than the one used in this study for quantifications, for demonstration only. The sclera canal was overexposed to highlight the LC beams. The *colors* represent local collagen fiber orientations which help discern the collagen structure. LC insertions are located at the edge where the LC beams join the sclera canal. We selected six regions to show the variations of LC insertions. Panel (**A**) contains an LC insertion beam perpendicular to the canal wall, whereas (**B**) contains a slanted insertion beam. Panel (**C**) contains more insertions than (**D**), meaning that the number and density of insertions vary from location to location. Panel (**E**) contains a wider insertion beam, whereas (**F**) contains a narrower insertion beam.

smooth, continuous location where the LC and sclera meet. The simplification is convenient for making gross measures of anatomy, and for making smooth continuum biomechanical models.[27–29] The approach, however, ignores that the LC itself has multiple elements, including collagenous LC beams and LC pores with neural tissues. Because the LC insertions are formed by collagen, the main load-bearing component of the LC, mechanical interactions between the LC and sclera must occur primarily through these discrete structures, and therefore to understand LC mechanics we must also understand the LC insertions. In this work, we will study the LC insertions understood as the discrete locations where collagenous LC beams meet the canal wall.

Investigative Ophthalmology & Visual Science

The complex nature of the LC-sclera interface is readily visible in images obtained using electron microscopy,[30,31] second harmonic generated imaging,[6,32] or polarized light microscopy[33,34] (Fig. 2). Recent OCT systems with adaptive optics reveal similar structures in vivo.[35] The LC insertions vary greatly in number, shape, and size. Some insertions resemble the wide roots of old trees, whereas others look much narrower. From the biomechanical perspective, a wider LC insertion may be able to support higher IOP-induced forces than a narrower LC insertion, providing stronger support to adjacent neural tissues and helping them bear higher levels of IOP. Similarly, a region with more or wider LC insertion beams may be more robust mechanically than a region with fewer or narrower beams. This suggests that sectorial variations in LC insertions number, size, and shape may contribute to the regional patterns in sensitivity to elevated IOP and of glaucoma development and progression.

To the best of our knowledge, the discrete nature of LC insertions has been largely ignored in studies of morphometry or biomechanics. Our goal was to test the hypothesis that the number, size, and shape of LC insertions are not uniform in-depth of LC or among quadrants. Specifically, we quantified four parameters of LC insertions: insertion width, number of insertions, insertion angle to the canal wall (90 degrees = perpendicular to the wall, and 0 degrees aligned with the wall), and insertion ratio (the fraction of LC periphery represented by LC beam insertions). The variations of LC insertions may lead to different LC robustness levels. Understanding the variations of LC insertions may help understand the patterns of neural tissue damage and visual impairment associated with glaucomatous vision loss.

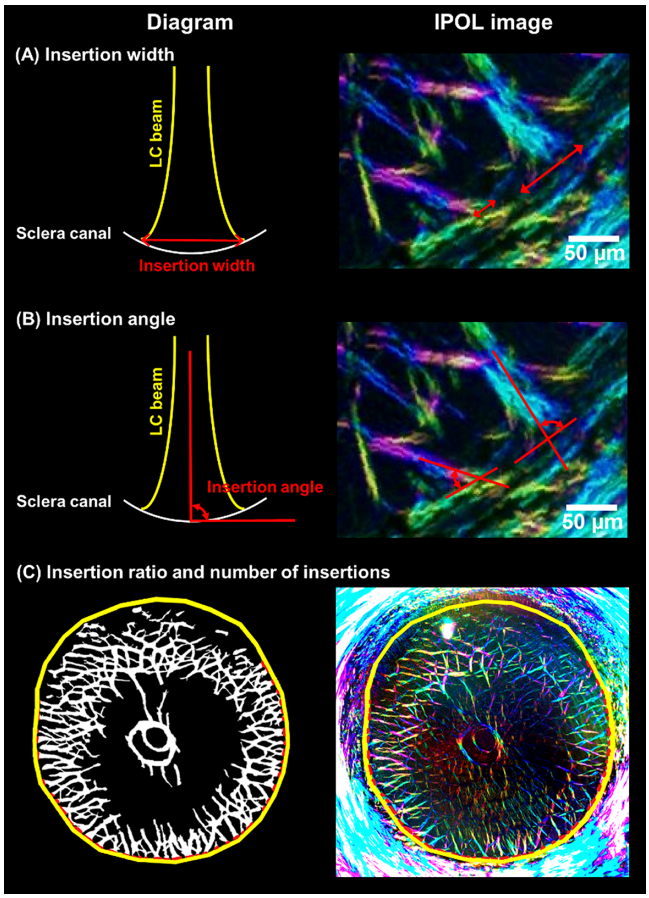

Figure 3. Definitions of insertion parameters. (*Left column*) Schematic diagrams and (*right column*) IPOL images showing the definition of insertion width, insertion angle, and insertion ratio. (**A**) (*left*) Insertion width was defined as the LC beam width at the sclera canal. (*Right*) Two LC insertions with different widths. The insertion width was quantified by marking with a straight line and calculating the length of the line. (**B**) (*left*) Insertion angle was defined as the angle between the LC beam and the tangent of sclera canal. (*Right*) Two LC insertions with different insertion angles. For each insertion angle, we marked the direction of the canal tangent and the LC beam with two straight lines. The insertion angle was calculated as the acute angle between the two lines. (**C**) (*left*) Insertion ratio was defined as the ratio between the area of insertions and the area of sclera canal. It was calculated as the ratio between the sum of all the insertion lengths (*red*) and the length of the canal opening at that depth (*yellow*). The number of insertions is the count of distinct LC insertion beams. (*Right*) Manual markings of the canal wall and the beam widths were overlayed on the IPOL image for demonstration.

Methods

Eye Procurement, Preparation, and Sectioning

The study was conducted in accordance with the tenets of the Declaration of Helsinki and the Association of Research in Vision and Ophthalmology's statement for the use of animals in ophthalmic and vision research. We used 6 eyes of adult female rhesus macaque monkeys (Macaca mulatta), 12 to 16 years of age. These eyes were originally acquired for use in other studies and were obtained from collaborators from animals that had been used for studies not involving the eyes. The eyes were ostensibly healthy, without known abnormalities, and obtained and processed within 6 hours of death. The globes were processed as described previously.[36–38] Briefly, the episcleral tissues, fat, and muscles were carefully removed. The globes were pressurized and immersion fixed in 10% formalin solution overnight. Because of the precious nature of primate tissues, we planned on these tissues to be useful for multiple studies. For this reason, the IOPs at fixation varied between 5 and 25 mm Hg. The consequences of this are addressed in the Discussion. After fixation, the ONH and posterior pole were excised with a circular trephine. The excised regions were cryosectioned coronally at 16 µm starting from the posterior side. Sections were collected without loss, starting when there was visible sclera and stopping when the canal was no longer visible.

Imaging and Registration

A set of sections completely enclosing the lamina was imaged for each eye. The number of sections varied between eyes depending on the curvature and thickness of the LC, and the tilt of the embedding. We then selected for analysis in this study the images of sections with visible LC insertions. This excluded from analysis images of sections without LC, or where the LC was only central, without LC insertions. This occurs, for example, in eyes with curved or bowed LCs. All told, every eye required 15 sections to be analyzed.

The selected sections, 15 sections from each eye, were imaged with the instant polarized light microscopy (IPOL) technique reported previously.[39,40] Briefly, the IPOL imaging system was developed on an inverted microscope (Olympus IX 83; Olympus, Tokyo, Japan) by retrofitting a polarization encoder in the illumination path and a polarization decoder in the imaging path. Each polarizer group consisted

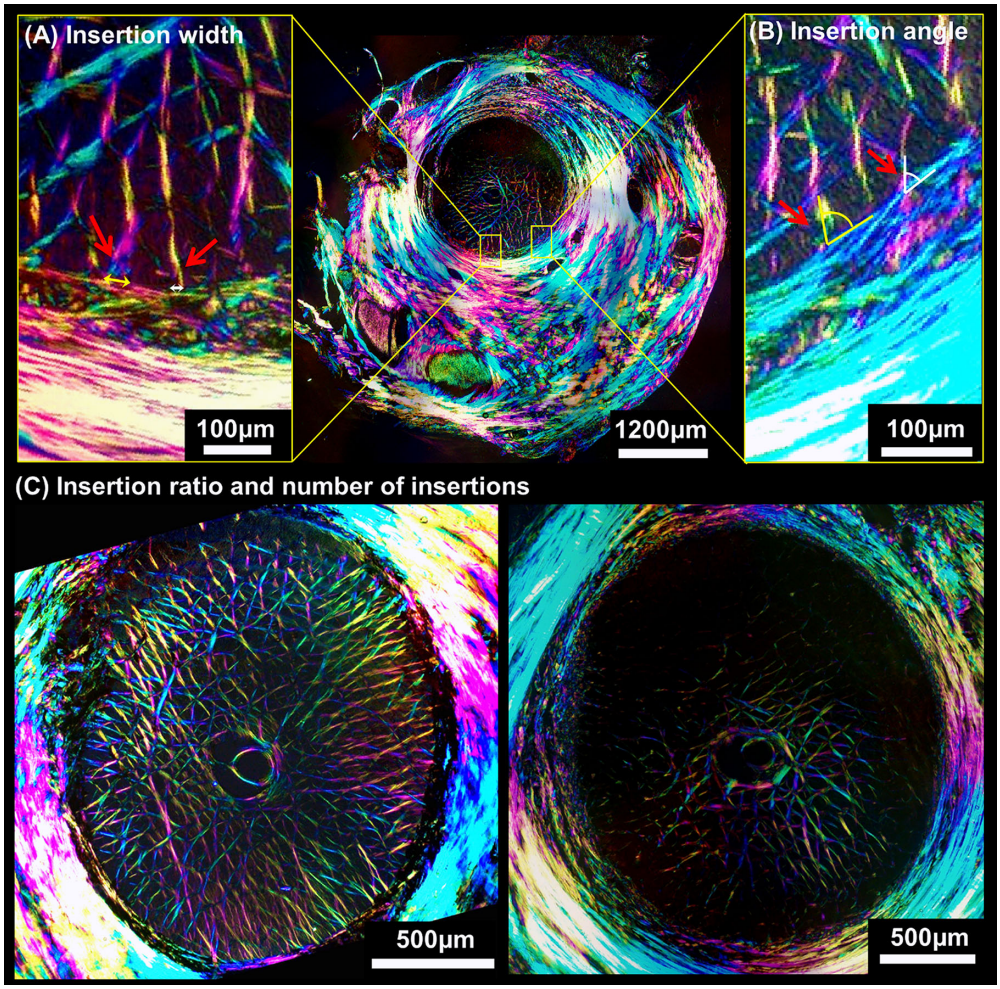

Figure 4. Variations of insertion parameters. Panel (**A**) shows two insertions with different insertion widths. (**B**) Shows two insertions with different insertion angles. (**C**) The two sections were selected from the same monkey eye. The left section was located closer to the midplane of LC and the right section was located closer to the posterior LC surface. The left section showed a greater number of insertions and a larger insertion ratio, whereas the right section contained significantly sparse insertions.

of a linear polarizer and a z-cut quartz plate. Linear polarizers in the polarization encoder and decoder were orientated orthogonally. A 4× strain-free objective (Olympus, Tokyo, Japan) was used for imaging (1.49 μm/pixel). Our implementation of IPOL includes image processing and quantification, and was based on an optical setup originally described elsewhere.[41]

The LC region appeared darker than the sclera, mainly due to the lower collagen density. Therefore, for imaging, we selected an exposure that highlighted LC beams and structure, even if it sometimes led to overexposure of the scleral tissues. The IPOL images displayed the collagen orientation and in-plane density in each pixel which helped better visualize the LC structure.[39,40] Because the sections were large, multiple images were captured (10% overlap) and stitched into mosaics to cover the whole section. Images from the same eye were stacked sequentially and registered to the most posterior image. The registration was done manually based on tissue edges and as described elsewhere.[42]

Insertion Quantification

We quantified four insertion parameters: insertion width, insertion angle, insertion ratio, and number of insertions (Fig. 3). Insertion width was defined as the width of the LC beam at the edge of the sclera canal. The insertion angle was the angle between the LC insertion beam and the tangent of the sclera canal. The insertion angle ranged from 0 degrees to 90 degrees. Ninety degrees indicated an LC insertion perpendicularly inserted into the canal wall, whereas 0 degrees meant the LC beam parallelly joined the canal. Insertion ratio was quantified as the ratio between the area of insertions and the area of LC periphery, with areas computed by width and section thickness. Number of insertions was the number of distinct LC beams inserted into the canal wall. The parameters were measured in each section in-depth of LC and in each quadrant (i.e. superior, inferior, nasal, and temporal).

The parameters were measured from lines drawn manually. All the manual markings in this section were done using FIJI is Just ImageJ (FIJI).[43,44] For insertion width, we marked the width using a straight line and calculated the length of the line. For the insertion angle, we marked two straight lines, indicating the direction of the LC beam and the direction of the local canal tangent, respectively. We calculated the acute angle between the two lines as the insertion angle. We counted the number of insertion width markings as the number of insertions. Here, we would like to note an impor-

tant consideration: when marking to get insertion widths, insertion angles, and counting the number of insertions, we compared the adjacent sections to avoid duplicate counting of the LC insertion beams that appeared in more than one section.

For insertion ratio, we manually marked along the edge of the sclera canal from each section, indicating the in-depth position and the quadrant. We re-marked the insertion widths following a similar procedure described above. Different from the method we used for quantifying insertion width, we marked the widths of all the LC insertion beams that were visible in a section, even though the same beam may appear in multiple sections. We calculated the insertion ratio as the sum of all LC beam widths divided by the perimeter of the canal. The calculations were done in MATLAB version 2022 (MathWorks, Natick, MA, USA).

Statistics

Linear mixed effect (LME) models, accounting for autocorrelations, or dependent similarities, between measurements from the same section, eye, and species, were used to assess if the parameters of insertions were associated with in-depth positions or quadrants.

Results

Examples of LC insertions with varying insertion widths, insertion angles, number of insertions, and insertion ratios are shown in Figure 4. Even when two insertion beams were close, they could differ significantly in width and angle, where one beam could be twice as wide as the other one, and the insertion angles differing by more than 10 degrees. Two sections located at different distances from the LC midplane showed significant differences in the number and density of insertions.

Insertions in the posterior LC were wider and with larger insertion angles than those in the anterior LC (P values $<$ 0.001; Fig. 5). In the most posterior LC, insertions widths were 38.56 $\pm$ 23.52 µm (mean $\pm$ SD) and insertion angles were 74.49 $\pm$ 11.65 degrees (mean $\pm$ SD). When looking through the LC depth from posterior to anterior, for every 16 µm, the insertion widths decreased by 1.29 µm (P $<$ 0.001), and the insertion angles decreased by 0.48 degrees (P $<$ 0.001). There were a greater number of insertions and

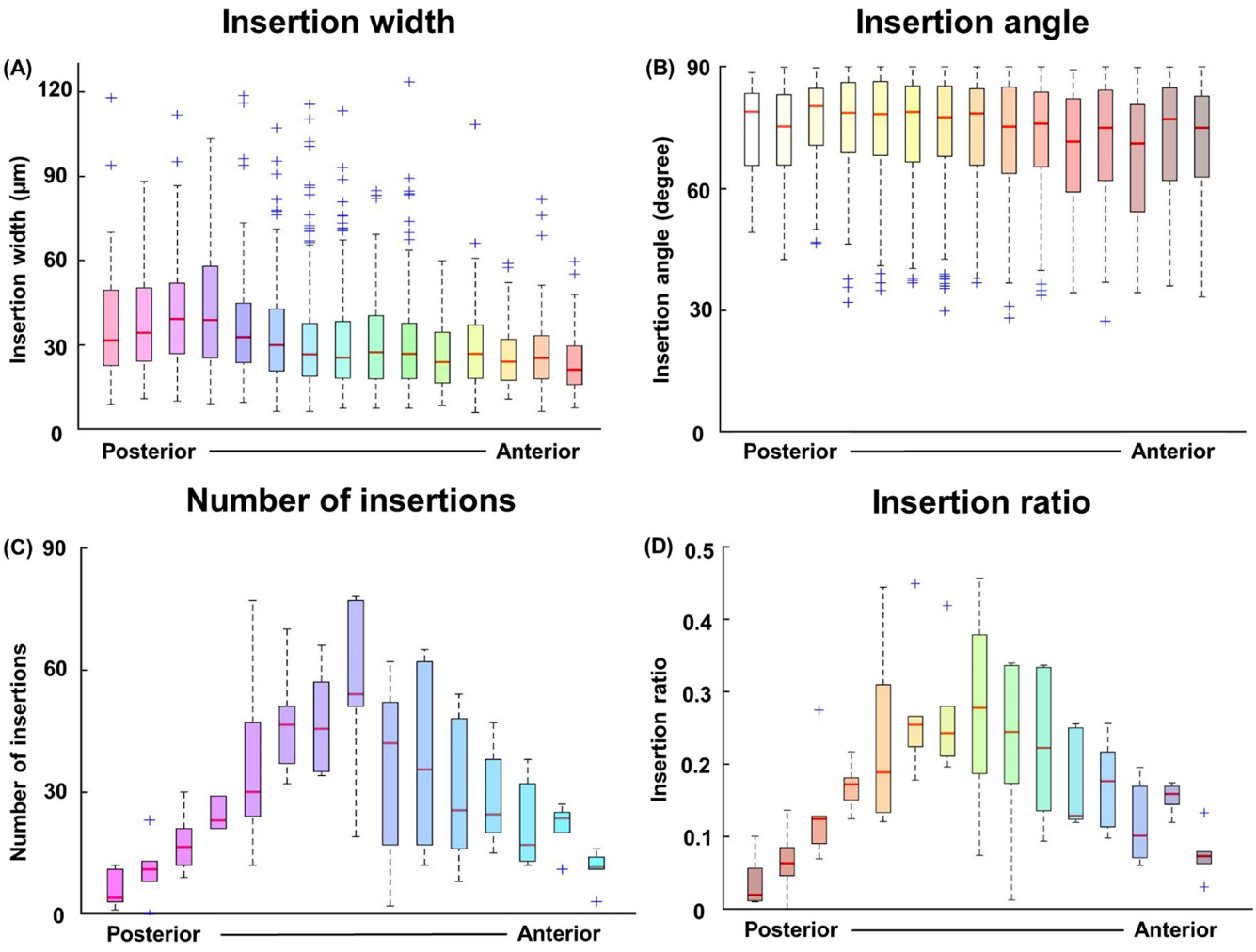

Figure 5. Variations of insertion width, insertion angle, number of insertions, and insertion ratio by depth. (**A, B**) Insertions in the most anterior LC were more slanted and significantly narrower than in the posterior LC (P values $<$ 0.001). (**C, D**) More insertions covered a larger ratio of the canal wall in the middle LC than in the anterior and posterior LC (P values $<$ 0.001).

Investigative Ophthalmology & Visual Science

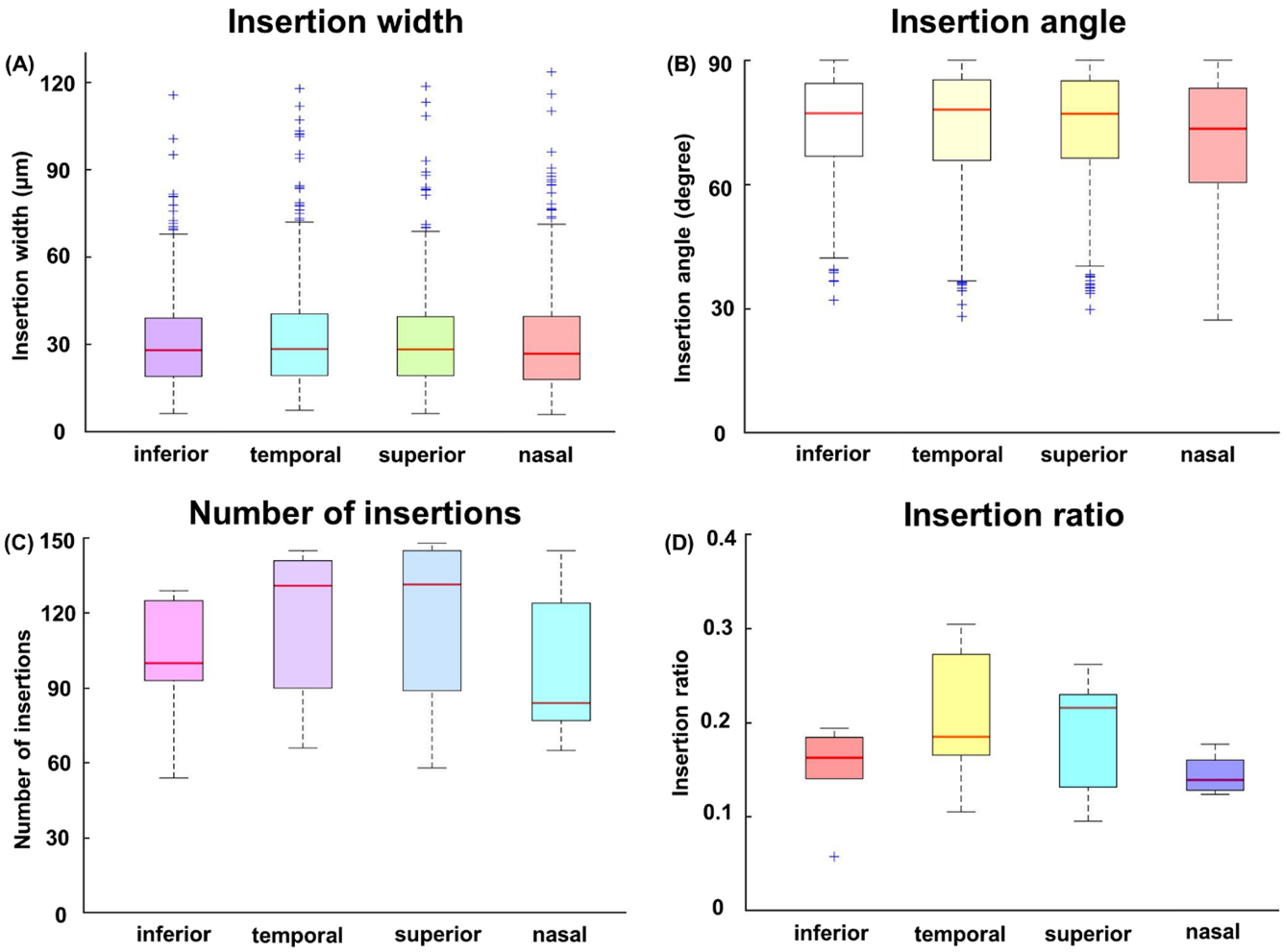

Figure 6. Variations of insertion width, insertion angle, number of insertions, and insertion ratio by quadrants. (**B**) Insertion angles in the nasal quadrant were significantly smaller than in the other quadrants ($P < 0.001$). (**A, C, D**) Insertion width, number of insertions, and insertion ratio were not significantly different among quadrants.

a larger insertion ratio in the middle LC than in the anterior and posterior LC (P values < 0.001). The section contained the maximum number of insertions and the largest insertion ratio was located at the midplane, having an average of 55 insertion beams and a 28% of insertion ratio.

In the nasal quadrant, insertion angles were 3.5 degrees significantly smaller than the other 3 quadrants ($P < 0.001$; Fig. 6). No significant differences in insertion width, ratio, and number were detected among quadrants.

The insertion widths and angles varied between individuals, yet, overall, the variations show similar behavior (Figs. 7, 8). The weakest trends were observed in the data for Monkey 1 OD. Each eye exhibited a relatively consistent pattern of insertion widths, number of insertions, and insertion ratios. Wider insertions were observed in the posterior LC compared to the anterior LC. Additionally, in every eye, the middle LC exhibited a higher number of insertions and insertion ratios compared to the anterior and posterior LC.

Results from the LME analysis indicate that there were differences between the animals (Fig. 9). For example, Monkey 4 OS had significantly smaller insertion widths. The differences were significant but small, as discernible in Figure 7.

Despite variations, the eye generally exhibited similar trends with maximal number of insertions and insertion ratio near the midplane. This can be discerned from the summary plots of number of insertions and ratio for all eyes as a function of depth and quadrant, shown in Figures 10 and 11, respectively. Monkey 1 OD had an interesting low number of insertions near the midplane, but this level was surrounded by planes with substantially higher measures. Variations between the quadrants were large without clear trends across the eyes.

The results of the LME tests within monkey eyes are summarized in plots and pair-wise comparison matrices shown in Figure 12. Considerable variations in insertion angles were observed across different eyes, indicating the absence of a consistent pattern valid for each individual eye. Similarly, the variations in insertion width, insertion ratio, and number of insertions among the quadrants were also substantial, and no clear pattern was detected that could be applied consistently to each eye. Furthermore, the insertion parameters from eyes belonging to the same animal were not found to be more similar compared to unrelated eyes.

On average, each monkey eye has 431 insertions ($\pm$ standard deviation = 75) with an insertion ratio of 0.1715 ($\pm$ standard deviation = 0.0315; see the Table).

Investigative Ophthalmology & Visual Science

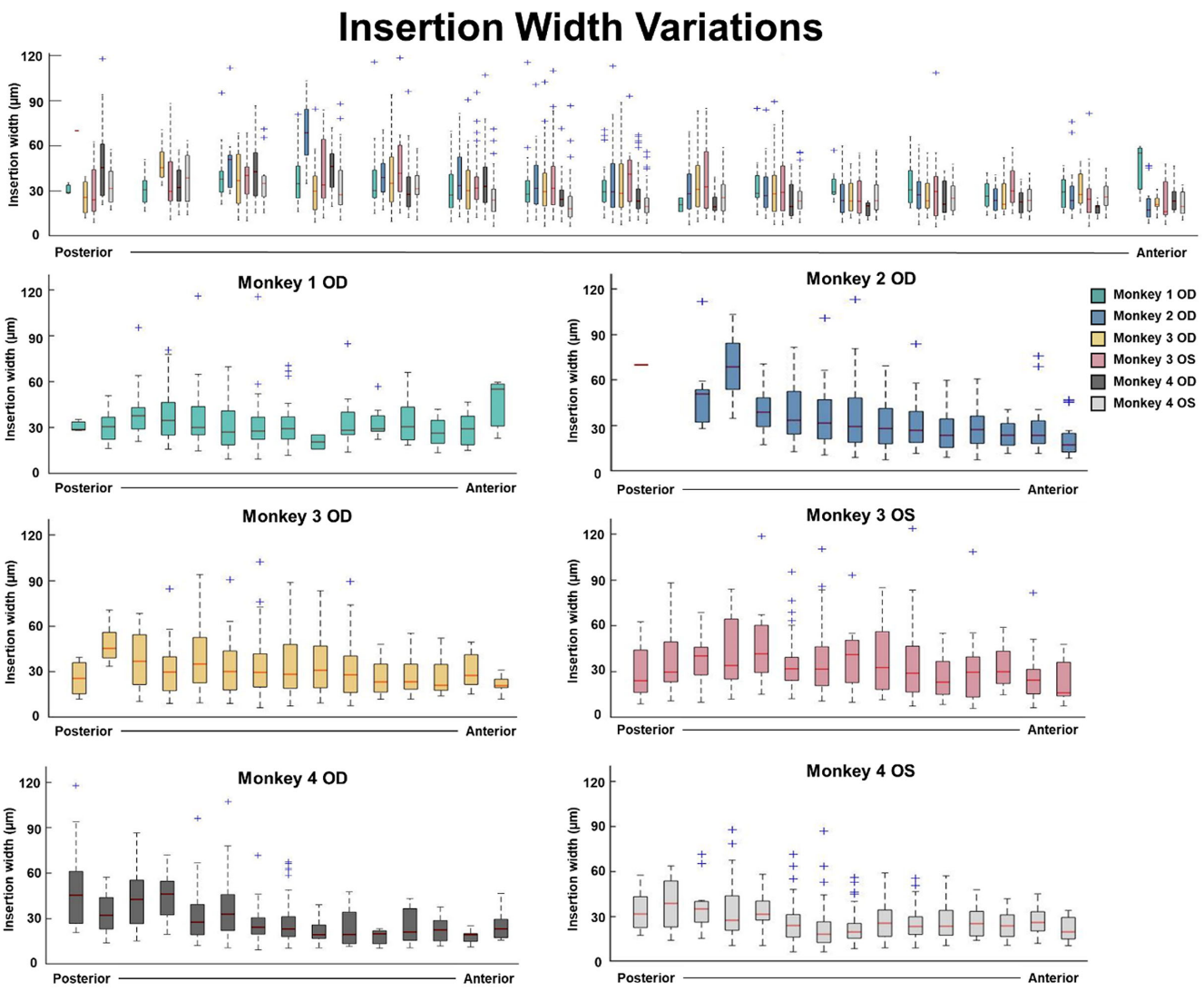

Figure 7. Insertion width variations from posterior LC to anterior LC in individual monkey eyes. The *top panel* illustrates the posterior-to-anterior insertion width changes across all six monkey eyes. The *bottom six panels* provide better visualization of the insertion widths for each eye. Notably, except for monkey 1 OD, the LC insertions in the posterior LC were wider compared to the anterior LC (P values < 0.01).

Discussion

Our goals were to acknowledge and better understand the discrete nature of LC insertions, carry out a systematic characterization of LC insertions in normal monkey eyes, and test the hypothesis that the shape and number of LC insertions vary in-depth through the LC and between quadrants. We characterized the LC insertions from six monkey eyes and quantified four parameters: insertion width, insertion angle, number of insertions, and insertion ratio. The variations of the parameters were compared through the LC depth and among the superior, inferior, nasal, and temporal quadrants. Three major results arise from this work. First, insertion widths were larger in the posterior LC than in the anterior LC. Second, the number of insertions and insertion ratios were larger in the sections closer to the LC midplane and were smaller in the sections closer to the LC anterior/posterior surface. Third, insertion angles were smaller in the anterior LC and in the nasal quadrant. We now discuss each of these results in more detail.

Insertion Widths Were Larger in the Posterior LC Than in the Anterior LC

It seems reasonable to think that a wider insertion beam may be stronger than a narrower insertion. Thus, our observation could indicate that the anterior LC may be weaker than the posterior LC. This potentially could contribute to the LC remodeling in the development of glaucoma. Increased IOP is the primary risk factor of glaucoma. Under chronic elevated IOP, two major changes have been observed, prelaminar neural tissue thinning and posterior (outward) migration of LC connective tissue.[12,25,45,46] The weaker anterior LC can be less robust to support the neural tissue under increased load compared to the posterior LC, thus contributing to the prelaminar neural tissue thinning. The weak anterior LC insertion beams may fail earlier in the development of glaucoma, resulting in the progressive posterior migration of LC connective tissue. This explanation is consistent with a common assumption made in many studies, arguing that IOP-related deformations cause acute failure of the

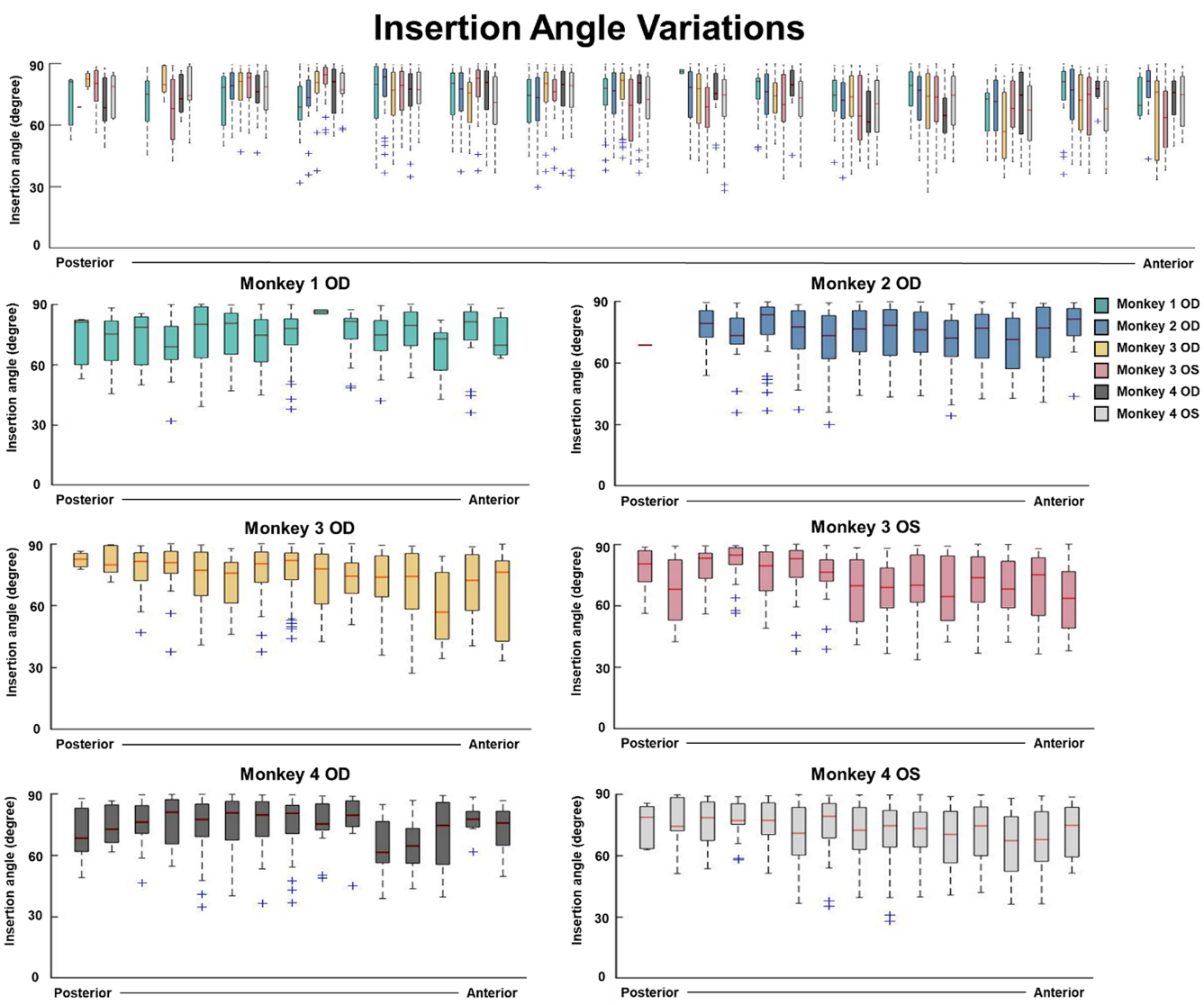

Figure 8. Insertion angle variations from posterior LC to anterior LC in individual monkey eyes. The *top panel* illustrates the posterior-to-anterior insertion angle changes across all six monkey eyes. The *bottom six panels* provide better visualization of the insertion angles for each eye. In monkey 3 OD, monkey 3 OS, and monkey 4 OS, the insertion angles were larger in the posterior LC than in the anterior LC (P values < 0.01).

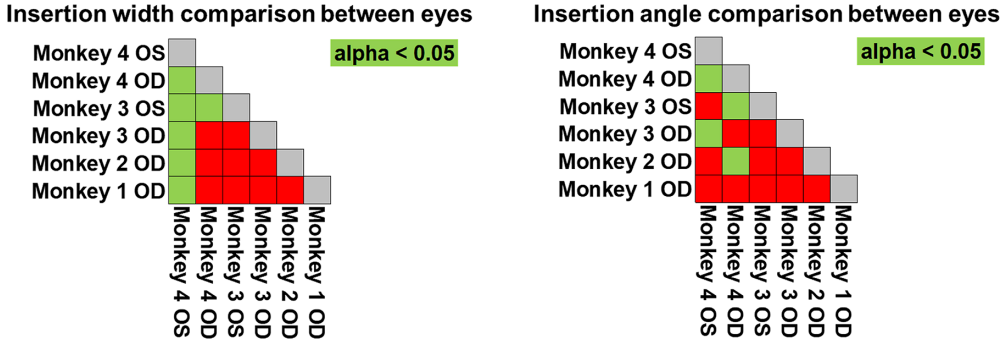

Figure 9. Matrix of LME tests doing pair-wise comparisons of (*left*) insertion widths and (*right*) insertion angles between eyes. Monkey 4 OS demonstrates significantly smaller insertion widths compared to other eyes (P values < 0.05). Additionally, significant differences in insertion angles reveal that monkey 4 OS has smaller insertion angles than monkey 3 OD and monkey 4 OD, whereas monkey 4 OD exhibits larger insertion angles than monkey 2 OD and monkey 3 OS (P values < 0.05).

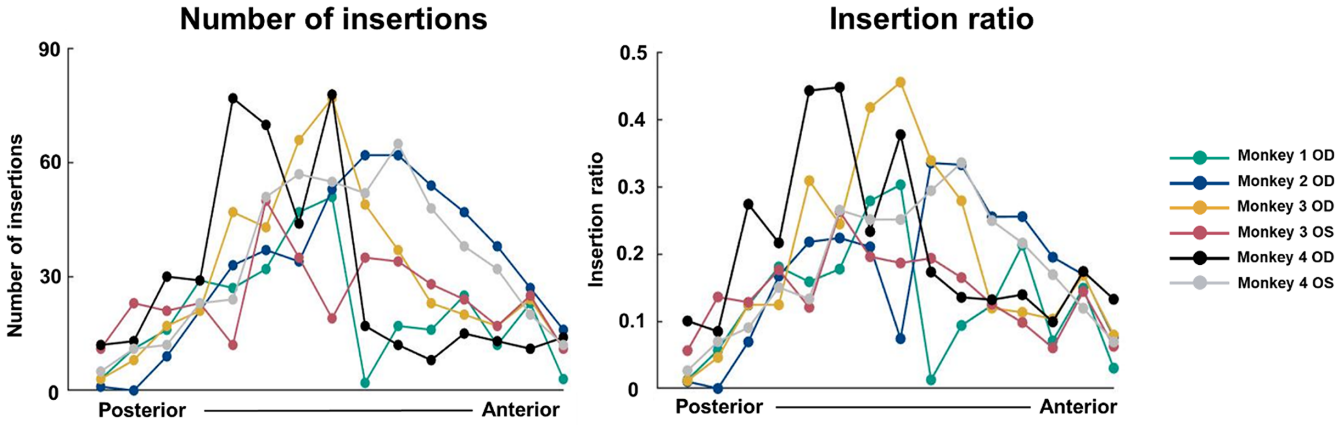

Figure 10. Line plots illustrating variations in the number of insertions (*left*) and insertion ratio (*right*) from posterior LC to anterior LC of each monkey eye. In every eye, the middle LC displays a greater number of insertions and larger insertion ratio in comparison to the anterior and posterior LC segments.

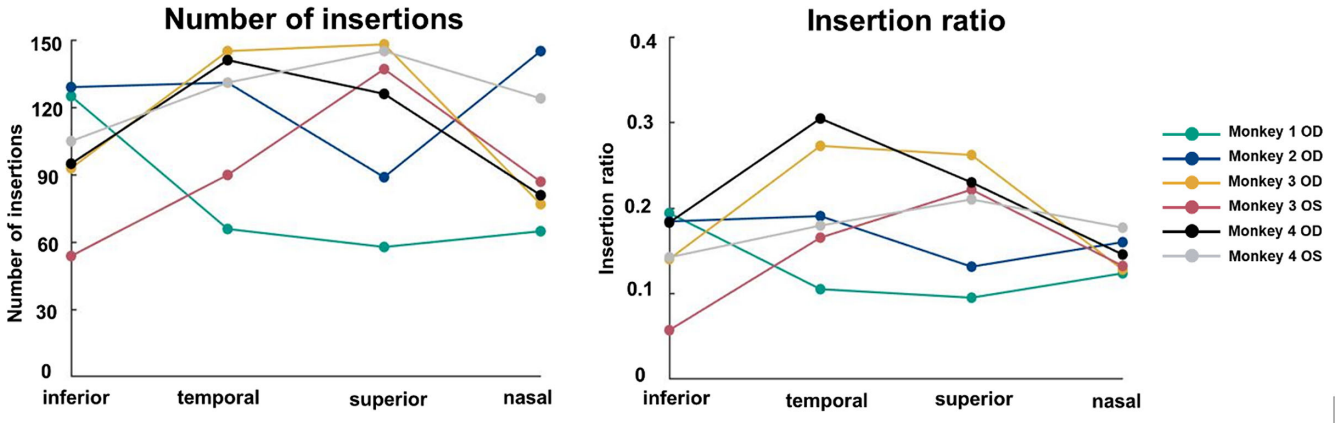

Figure 11. Line plots illustrating variations in the number of insertions (*left*) and insertion ratio (*right*) across the four quadrants of each monkey eye.

anterior laminar beams, thereby transferring load to adjacent beams in a cascade of damage that results in the glaucomatous cupping.[7,8,47,48] A failing or disappearing beam may not provide adequate support to resident or adjacent capillaries, potentially also explaining the appearance of hemorrhages at the LC periphery early in glaucoma.[49] Nevertheless, we should also consider that LC collagen and insertions are complex living elements and that what we describe as failure is unlikely to be as in the conventional mechanical sense of reaching an ultimate stress. If an elevated IOP causes abnormally high stresses on the anterior LC insertions, these could remodel to strengthen. Simulations of the biomechanical role of LC location and shape on IOP-related stresses suggest that a deeper and more curved LC results in lower stresses within the LC. The LC deepening could be the result of anterior LC insertion failing or a process of resorption.[3,8,12,21,25,50]

The Number of Insertions and Insertion Ratios Were Larger With Greater Variability in Sections Closer to the LC Midplane and Smaller in the Sections Closer to the LC Anterior/Posterior Surface

These variations could impact how forces and deformations are transmitted between the sclera canal and LC. The discrete LC beam insertions may imply that the interactions between LC and surrounding load-bearing tissues are nonlinear and discontinuous over the canal, with forces concentrated in where the LC beams are inserted into the canal. Regions with more beams and a larger portion of LC periphery attached to the canal wall may imply that these regions are stronger in supporting the neural tissues. However, due to the lack of information about LC insertion microstructure, number of insertions, and insertion ratios were not considered previously. Instead, when modeling the ONH biomechanics, it was commonly assumed that the LC and LC insertions are continuum structures that span 100% of the canal perimeter.[25,51–53] In fact, only 20 to 40 percent of the canal perimeter area is connected by LC beams. Given the strong effect of sclera characteristics on LC mechanics,[54–56] future studies should look into potential associations between the anterior-posterior variations in LC beam insertions and the architecture and mechanics of the peripapillary sclera. Ignoring the variations of number of insertions and insertion ratio may obfuscate efforts to understand the interactions between the LC and the surrounding loading-bearing tissues, which could, in turn, impair our understanding of the biomechanical robustness of the LC and sensitivity to elevated IOP (Fig. 13).[8,10,11,13] Thus, it is important to consider these two parameters in numerical models, and future study is important to explore their biomechanical roles.

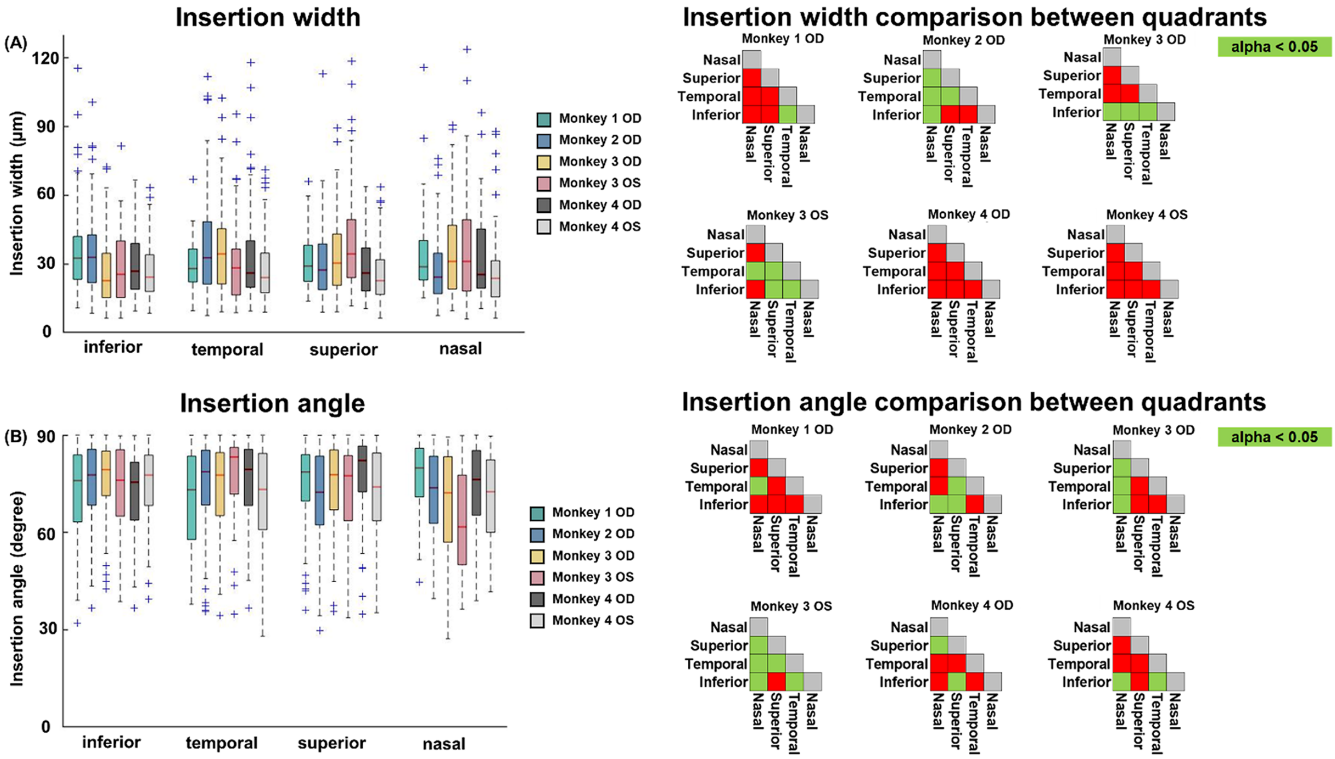

Figure 12. Variations in (**A**) insertion width and (**B**) insertion angle among each monkey eye. The matrix of LME tests illustrates pair-wise comparisons of these parameters between quadrants.

Table. Number of Insertions and Insertion Ratio in the Whole LC Region of Individual Monkey Eyes

	Number of Insertions	Insertion Ratio
Monkey 1 OD	314	0.1318
Monkey 2 OD	494	0.1681
Monkey 3 OD	463	0.1972
Monkey 3 OS	368	0.1421
Monkey 4 OD	443	0.2142
Monkey 4 OS	505	0.1756

On average, the number of insertions in each monkey eye was found to be 431 (± standard deviation of 75), with an insertion ratio of 0.1715 (± standard deviation of 0.0315).

Insertion Angles Were Smaller in the Anterior LC Than in the Posterior LC

Insertion angles in the nasal quadrant were also found smaller than in the other three quadrants. A 90-degrees insertion angle means a radially oriented LC insertion beam, whereas a 0 degrees small insertion angle means an LC beam tangentially inserted into the canal wall. The orientation of the LC insertions can affect the behavior of the most peripheral LC beams and pores, in turn affecting neural tissues within.[3,53] For instance, more tangentially aligned LC insertion beams are more likely to rotate with canal expansion and causing shear and compression within the pores that could contribute to neural tissue loss. In regions with more radial insertions, canal expansion is less likely to cause insertion beam rotation, which could be better for the neural tissues. Conversely, radial insertions will likely bear larger stresses during canal expansion or bowing, which could trigger collagen remodeling. Although the above hypotheses seem reasonable, the observed quadrant variations of insertion angles do not fully explain reports of regional susceptibility, which have shown that inferior-temporal and superior-temporal quadrants of the ONH are more susceptible to damage in early glaucoma.[23,57] This could be because insertion angles have other implications that are yet to be understood. If LC insertion mechanics vary with the insertion angle, then it is possible that the protection that the LC insertion provides to a capillary within also varies with the angle. For instance, it is possible that LC insertions with small angles are less capable of providing the necessary structural support to a capillary within than insertions at large angles. Further work is necessary to understand the biomechanical role of insertion angles.

Studies treating the LC insertion as a smooth continuum have reported that the LC sometimes inserts into the pia mater, and not only on the sclera as it had traditionally been thought. This was first described in the human model and later confirmed in a monkey model of experimental glaucoma. By leveraging the strengths of the monkey models to distinguish control versus experimental eyes and carefully systematic block-face histomorphometry, the investigators were able to demonstrate that healthy young eyes did not exhibit LC insertion into the pia. LC insertion into the pia appeared first in eyes with early glaucoma, and increased as the pathology progressed. In some eyes with advanced glaucoma in some quadrants, the LC was almost entirely inserted into the pia. The concurrent progressive increase in LC insertion into the pia mater and the deeper location of the anterior LC insertion limit was summarized as an IOP-induced "posterior (outward) migration of the LC and early cupping in monkey experimental glaucoma."[12] A later study in humans reported that LC insertion into the

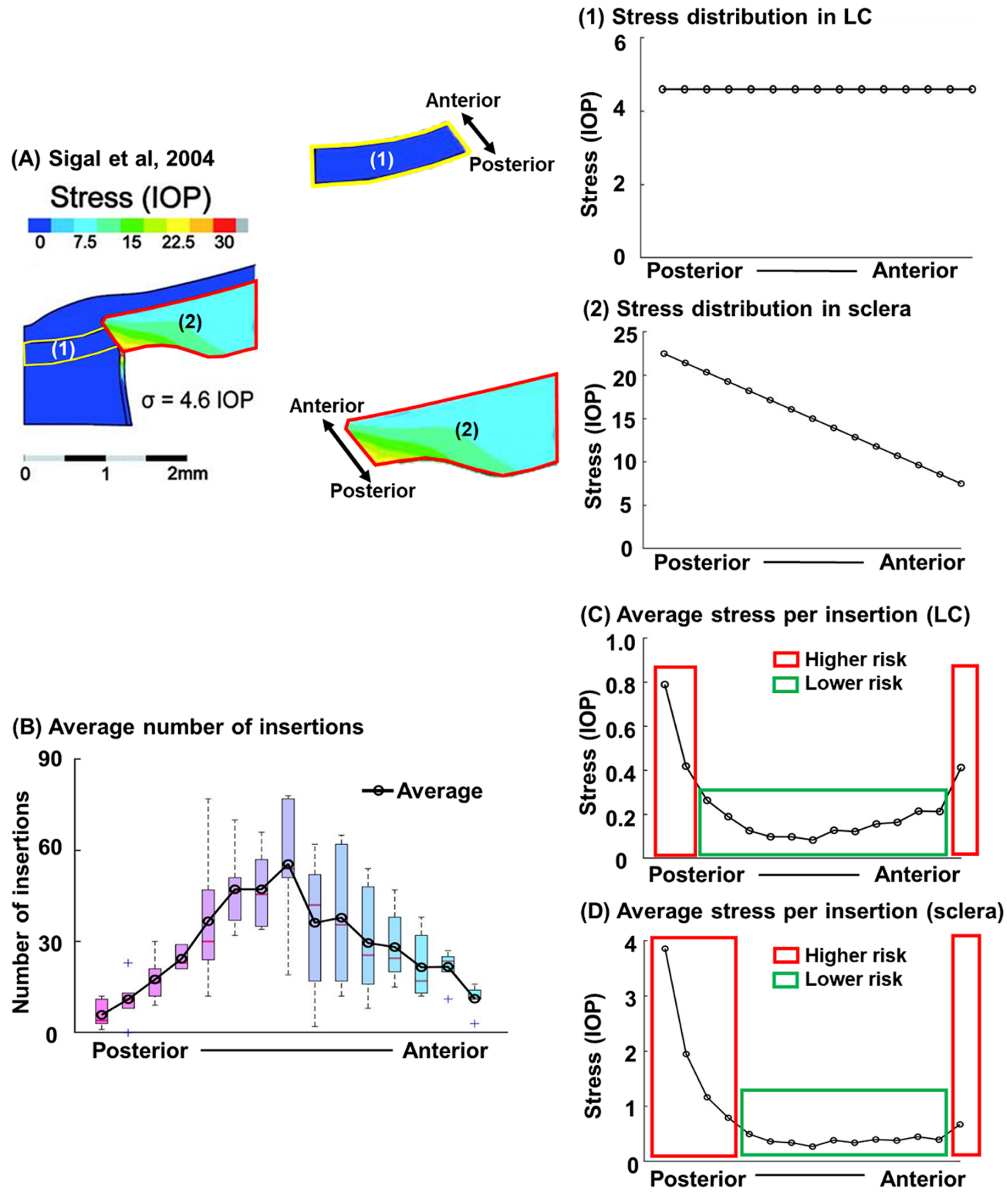

Figure 13. Impact of the variation number of insertions with depth on the ONH stress distribution. (**A**) Adapted from Sigal et al., 2004, this figure demonstrates the von Mises equivalent stress of the ONH region under an IOP of 50 mm Hg. The stress is presented as multiples of IOP, providing insights into the forces acting within the tissue. The LC (*region outlined by the yellow line*) interacts with the sclera (*region outlined by the red line*) through LC insertions. (1) The stress within the LC region is relatively uniform at 4.6 IOP, whereas (2) the stress at the scleral canal edge varies from 7.5 IOP to 22.5 IOP from anterior to posterior. (**B**) The number of insertions across the six monkey eyes, spanning from the posterior LC to the anterior LC. *Box plots* illustrate the variations, whereas the *black line* represents the average number of insertions at different depths. (**C**) In contrast to the continuum approach in panel (**A**), where LC insertions were treated as a continuum, considering the average stress acting through the LC and borne by each insertion reveals significantly higher stress per insertion beam at the posterior and anterior LC surfaces. Thus, the LC insertions at the posterior and anterior LC surfaces (*red rectangles*) can subject to higher risk of damage compare to insertions at mid-plane of the LC (*green rectangles*). (**D**) Similarly, by assessing the average stress acting through the scleral tissue and borne by each insertion, it becomes evident that the average stress per insertion beam is 8 times higher in the posterior LC compared to the mid-plane of the LC. Consequently, the LC beams located at the posterior and anterior surfaces (*red rectangles*) may face a higher risk of damage when subjected to increased IOP. Such critical information is not available if we study the LC insertions as a continuum. In this analysis, we considered only the number of insertions, and not their width. As shown in Figure 5, LC insertion width decreases from the maximum at the posterior LC to minimum at the anterior LC. The wider posterior LC insertions may be better able to bear the higher loads, but this may not be the case for the more narrow anterior LC insertions.

pia mater is common in middle-aged and older eyes, and does not increase with age, at least after 65 years old.[13] More recent studies using OCT have provided extensive indirect evidence in support of the concept of the progressive migration of the LC, but the difficulty in directly visualizing the peripheral LC has meant that the LC insertions remain relatively poorly characterized compared with other aspects of the LC, like curvature and depth.[58–60] Development of more sensitive OCTs and better image post-processing tools may eventually allow proven accurate measurement of LC insertions in vivo.[14,15,35,61] In the meantime, histological analysis remains a reasonable approach. Although not a core goal

of this work, a quick review of the images did not reveal any clear indication of LC insertions into the pia. This seems reasonable as the tissues came from young normal monkey eyes.

LC insertions have complicated shapes. Hence, the question could arise if the measurements may depend on the imaging resolution. A lower resolution allows for faster imaging (less images per mosaic) and more prompt file handling due to lower memory and storage needs. The study was conducted based on images with a resolution of 1.49 µm/pixel. To evaluate the effect of the resolution, we imaged again the sections of 2 monkey eyes with a resolution of 0.66 µm/pixel. We then marked the insertions twice on different days on both low and high resolution images. We compared the parameters of insertions obtained and found that there was no statistically significant difference. This is consistent with a previous study on which we evaluated the role of magnification on the results from polarized light microscopy.[37]

It is important to consider the limitations of this study. First, we quantified the LC insertions only in the monkey. Monkey and human LCs are different in geometry, where previous studies have reported the difference in LC shape and insertion widths between the two species.[33,62] Thus, the results of this study have limited application to human eyes. We position that it is important to understand the monkey as an animal model.[63,64] In future studies, it will be necessary to study LC insertions in other animal models and in human eyes.

Second, when mounting the ONH sample for sectioning, we leveled the LC surface and made it parallel to the sectioning plane. However, it was still possible that the LC surface was tilted at an angle relative to the sectioning plane, which could influence the measurements of the in-depth variations. We quantified the angle of tilting from the 6 eyes and found that the average tilted angle was 3.1 degrees, which was small and should not cause significant impact on the measurements. In the future, it would be beneficial to come up with advanced image processing methods to resolve the issue of tilting when needed.

Third, the tissues analyzed had been fixed, sectioned, and images, and the images digitally processed to form stacks from which the measurements were taken. It is possible that this processing could have distorted the tissues. Elsewhere, we have shown that our tissue processing for polarized light based on formalin fixation and cryosectioning does not cause significant or substantial shrinkage or deformations.[65] Any distortions seem more likely to affect LC insertion shape and angle than width or ratio. There are other potential effects of our use of sections. Although we checked to avoid counting large insertions appearing in multiple sections as different insertions, the methodology is imperfect. Errors would likely lead to overestimating counts and underestimating size. We also were unable to measure the precise 3D size of an insertion, approximating by a rectangular shape (width by thickness). This could overestimate insertion size, particularly of insertions thinner than the sectioning thickness.

Fourth, the monkey eyes were pigmented. Although not as extensive as in other species, such as pigs, pigments are excellent at absorbing light and block the signal used for IPOL.[37] This could have resulted in us missing some insertions, because pigment tends to be more prominent in the anterior LC this could have affected the results. Because of the low energy in white light used for IPOL there is no risk of absorption causing heating or tissue damage, as it can happen with second harmonic generated microscopy.[66] On the other hand, second harmonic generated microscopy can provide depth information not available to our IPOL implementation.[5,67,68] Future polarization-sensitive second harmonic generation may be able to integrate the strengths of both techniques.[69,70]

Fifth, we characterized the LC insertions using fairly simple parameters. This was convenient for a first approach, but it does not provide a full accounting of the extremely complicated nature of these structures. Future studies could use more sophisticated techniques, for instance, from geometric morphometrics,[71,72] to characterize LC insertion shapes with greater detail. Another potential interesting area of research would be to analyze carefully the organization of the collagen on the scleral side of the insertions to determine their microstructure and better understand their biomechanics.[73,74]

Sixth, the eyes were fixed at different IOPs between 5 and 25 mm Hg. This difference is expected to alter the collagen microstructure, including the degree of fiber undulations or crimp,[36,75] and cause distortions and deformations of the whole ONH.[20,52,76] Nevertheless, the deformations are unlikely to be large enough to have substantial effects on the width and ratio of the LC insertions.[32,77] Although it is possible that large changes in IOP could affect LC depth, for example, through bowing,[78,79] such rotations of the scleral wall are most pronounced in the longitudinal plane and thus likely have only minor effects on the coronal angles measured in this work. Because the pressures are far below any that could cause tissue failure and the pressurization was done after death, we would not expect changes in the number or location of the LC insertions.

It is also important for readers to consider that our results were based on six eyes from four monkeys. It is impossible to know whether the results from this relatively small sample represent, or not, a larger population. This is even more marked given the known wide variability in LC morphology and architecture.[5,20,80]

In conclusion, we have characterized the insertion width, insertion angle, number of insertions, and insertion ratio in normal monkey LC. We found substantial and significant variations of LC insertions in-depth of LC and among quadrants. Different shapes and varying number of LC insertions may represent different levels of robustness of the LC periphery. Understanding these differences potentially could contribute to a better understanding of the regional susceptibilities to glaucomatous damage.

Acknowledgments

Supported by the National Institutes of Health R01-EY031708, R01-EY023966, P30-EY008098, and T32-EY017271 (Bethesda, MD, USA), the Eye and Ear Foundation (Pittsburgh, PA, USA), and Research to Prevent Blindness (unrestricted grant to UPMC Ophthalmology, and Stein innovation award to I. A. Sigal).

Disclosure: **F. Ji**, None; **M.R. Islam**, None; **B. Wang**, None; **Y. Hua**, None; **I.A. Sigal**, None

References

1. Quigley HA, Flower RW, Addicks EM, McLeod DS. The mechanism of optic nerve damage in experimental acute intraocular pressure elevation. *Invest Ophthalmol Vis Sci*. 1980;19:505–517.

2. Hernandez MR. The optic nerve head in glaucoma: role of astrocytes in tissue remodeling. *Prog Retin Eye Res*. 2000;19:297–321.
3. Roberts MD, Sigal IA, Liang Y, Burgoyne CF, Downs JC. Changes in the biomechanical response of the optic nerve head in early experimental glaucoma. *Invest Ophthalmol Vis Sci*. 2010;51:5675–5684.
4. Sigal IA, Flanagan JG, Tertinegg I, Ethier CR. Finite element modeling of optic nerve head biomechanics. *Invest Ophthalmol Vis Sci*. 2004;45:4378–4387.
5. Behkam R, Kollech HG, Jana A, et al. Racioethnic differences in the biomechanical response of the lamina cribrosa. *Acta Biomater*. 2019;88:131–140.
6. Ling YTT, Shi R, Midgett DE, Jefferys JL, Quigley HA, Nguyen TD. Characterizing the collagen network structure and pressure-induced strains of the human lamina cribrosa. *Invest Ophthalmol Vis Sci*. 2019;60:2406–2422.
7. Sigal IA, Ethier CR. Biomechanics of the optic nerve head. *Exp Eye Res*. 2009;88:799–807.
8. Burgoyne CF, Downs JC, Bellezza AJ, Suh JK, Hart RT. The optic nerve head as a biomechanical structure: a new paradigm for understanding the role of IOP-related stress and strain in the pathophysiology of glaucomatous optic nerve head damage. *Prog Retin Eye Res*. 2005;24:39–73.
9. Wang X, Beotra MR, Tun TA, et al. In vivo 3-dimensional strain mapping confirms large optic nerve head deformations following horizontal eye movements. *Invest Ophthalmol Vis Sci*. 2016;57:5825–5833.
10. Sigal IA. Interactions between geometry and mechanical properties on the optic nerve head. *Invest Ophthalmol Vis Sci*. 2009;50:2785–2795.
11. Jonas JB, Jonas SB, Jonas RA, Holbach L, Panda-Jonas S. Histology of the parapapillary region in high myopia. *Am J Ophthalmol*. 2011;152:1021–1029.
12. Yang H, Williams G, Downs JC, et al. Posterior (outward) migration of the lamina cribrosa and early cupping in monkey experimental glaucoma. *Invest Ophthalmol Vis Sci*. 2011;52:7109–7121.
13. Sigal IA, Flanagan JG, Lathrop KL, Tertinegg I, Bilonick R. Human lamina cribrosa insertion and age. *Invest Ophthalmol Vis Sci*. 2012;53:6870–6879.
14. Girard MJ, Tun TA, Husain R, et al. Lamina cribrosa visibility using optical coherence tomography: comparison of devices and effects of image enhancement techniques. *Invest Ophthalmol Vis Sci*. 2015;56:865–874.
15. Kim YW, Jeoung JW, Girard MJ, Mari JM, Park KH. Positional and curvature difference of lamina cribrosa according to the baseline intraocular pressure in primary open-angle glaucoma: a swept-source optical coherence tomography (SS-OCT) study. *PLoS One*. 2016;11:e0162182.
16. Kim YW, Jeoung JW, Kim DW, et al. Clinical assessment of lamina cribrosa curvature in eyes with primary open-angle glaucoma. *PLoS One*. 2016;11:e0150260.
17. Kim Y, Kim D, Jeoung J, Kim D, Park K. Peripheral lamina cribrosa depth in primary open-angle glaucoma: a swept-source optical coherence tomography study of lamina cribrosa. *Eye*. 2015;29:1368–1374.
18. Lee KM, Kim T-W, Weinreb RN, Lee EJ, Girard MJ, Mari JM. Anterior lamina cribrosa insertion in primary open-angle glaucoma patients and healthy subjects. *PLoS One*. 2014;9:e114935.
19. Yang H, Williams G, Downs J, et al. Optic nerve head (ONH) lamina cribrosa insertion migration and pialization in early non-human primate (NHP) experimental glaucoma. *Invest Ophthalmol Vis Sci*. 2010;51:1631.
20. Sigal IA, Flanagan JG, Tertinegg I, Ethier CR. 3D morphometry of the human optic nerve head. *Exp Eye Res*. 2010;90:70–80.
21. Downs JC, Roberts MD, Sigal IA. Glaucomatous cupping of the lamina cribrosa: a review of the evidence for active progressive remodeling as a mechanism. *Exp Eye Res*. 2011;93:133–140.
22. Takusagawa HL, Hoguet A, Junk AK, Nouri-Mahdavi K, Radhakrishnan S, Chen TC. Swept-source OCT for evaluating the lamina cribrosa: a report by the American Academy of Ophthalmology. *Ophthalmology*. 2019;126:1315–1323.
23. Kiumehr S, Park SC, Dorairaj S, et al. In vivo evaluation of focal lamina cribrosa defects in glaucoma. *Arch Ophthalmol*. 2012;130:552–559.
24. Grytz R, Meschke G, Jonas JB. The collagen fibril architecture in the lamina cribrosa and peripapillary sclera predicted by a computational remodeling approach. *Biomech Model Mechanobiol*. 2011;10:371–382.
25. Grytz R, Sigal IA, Ruberti JW, Meschke G, Crawford Downs J. Lamina cribrosa thickening in early glaucoma predicted by a microstructure motivated growth and remodeling approach. *Mech Mater*. 2012;44:99–109.
26. Sigal IA, Yang H, Roberts MD, Burgoyne CF, Downs JC. IOP-induced lamina cribrosa displacement and scleral canal expansion: an analysis of factor interactions using parameterized eye-specific models. *Invest Ophthalmol Vis Sci*. 2011;52:1896–1907.
27. Sigal IA, Flanagan JG, Tertinegg I, Ethier CR. Predicted extension, compression and shearing of optic nerve head tissues. *Exp Eye Res*. 2007;85:312–322.
28. Wang X, Rumpel H, Lim WEH, et al. Finite element analysis predicts large optic nerve head strains during horizontal eye movements. *Invest Ophthalmol Vis Sci*. 2016;57:2452–2462.
29. Grytz R, Krishnan K, Whitley R, et al. A meshfree approach to incorporate complex anisotropic and heterogeneous material properties into eye-specific finite element models. *Comput Methods Appl Mech Eng*. 2020;358:112654.
30. Quigley HA, Addicks EM. Regional differences in the structure of the lamina cribrosa and their relation to glaucomatous optic nerve damage. *Arch Ophthalmol*. 1981;99:137–143.
31. Jonas J, Mardin CY, Schlötzer-Schrehardt U, Naumann G. Morphometry of the human lamina cribrosa surface. *Invest Ophthalmol Vis Sci*. 1991;32:401–405.
32. Sigal IA, Grimm JL, Jan N-J, Reid K, Minckler DS, Brown DJ. Eye-specific IOP-induced displacements and deformations of human lamina cribrosa. *Invest Ophthalmol Vis Sci*. 2014;55:1–15.
33. Ji F, Yang B, Hua Y, Lee P-Y, Zhu Z, Sigal IA. Characterization of lamina cribrosa beam insertion into the sclera canal in sheep, pig, monkey, and human. *Invest Ophthalmol Vis Sci*. 2020;61:4782–4782.
34. Ji F, Lam P, Brazile BL, Hua Y, Sigal IA. Variations in lamina cribrosa insertions into the sclera may contribute to regional differences in neural tissue damage and sensitivity to elevated intraocular pressure. *Invest Ophthalmol Vis Sci*. 2023;64:61.
35. Shiga Y, Nishida T, Jeoung JW, Di Polo A, Fortune B. Optical coherence tomography and optical coherence tomography angiography: essential tools for detecting glaucoma and disease progression. *Front Ophthalmol (Lausanne)*. 2023;3:1217125.
36. Jan N-J, Gomez C, Moed S, et al. Microstructural crimp of the lamina cribrosa and peripapillary sclera collagen fibers. *Invest Ophthalmol Vis Sci*. 2017;58:3378–3388.
37. Jan N-J, Grimm JL, Tran H, et al. Polarization microscopy for characterizing fiber orientation of ocular tissues. *Biomed Opt Express*. 2015;6:4705–4718.

Investigative Ophthalmology & Visual Science

38. Jan N-J, Lathrop K, Sigal IA. Collagen architecture of the posterior pole: high-resolution wide field of view visualization and analysis using polarized light microscopy. *Invest Ophthalmol Vis Sci*. 2017;58:735–744.
39. Yang B, Lee PY, Hua Y, et al. Instant polarized light microscopy for imaging collagen microarchitecture and dynamics. *J Biophotonics*. 2021;14:e202000326.
40. Lee P-Y, Yang B, Hua Y, et al. Real-time imaging of optic nerve head collagen microstructure and biomechanics using instant polarized light microscopy. *Exp Eye Res*. 2022;217:108967.
41. Shribak M. Polychromatic polarization microscope: bringing colors to a colorless world. *Sci Rep*. 2015;5:17340.
42. Gogola A, Jan N-J, Lathrop KL, Sigal IA. Radial and circumferential collagen fibers are a feature of the peripapillary sclera of human, monkey, pig, cow, goat, and sheep. *Invest Ophthalmol Vis Sci*. 2018;59:4763–4774.
43. Schindelin J, Arganda-Carreras I, Frise E, et al. Fiji: an open-source platform for biological-image analysis. *Nat Methods*. 2012;9:676–682.
44. Preibisch S, Saalfeld S, Tomancak P. Globally optimal stitching of tiled 3D microscopic image acquisitions. *Bioinformatics*. 2009;25:1463–1465.
45. Burgoyne C. The morphological difference between glaucoma and other optic neuropathies. *J Neuroophthalmol*. 2015;35(Suppl 1):S8–S21.
46. Kim DW, Jeoung JW, Kim YW, et al. Prelamina and lamina cribrosa in glaucoma patients with unilateral visual field loss. *Invest Ophthalmol Vis Sci*. 2016;57:1662–1670.
47. Downs JC, Roberts MD, Burgoyne CF. The mechanical environment of the optic nerve head in glaucoma. *Optom Vis Sci*. 2008;85:425.
48. Jonas JB, Berenshtein E, Holbach L. Lamina cribrosa thickness and spatial relationships between intraocular space and cerebrospinal fluid space in highly myopic eyes. *Invest Ophthalmol Vis Sci*. 2004;45:2660–2665.
49. Park H-YL, Lee J, Jung Y, Park CK. Optic disc hemorrhage and lamina cribrosa defects in glaucoma progression. *Sci Rep*. 2017;7:3489.
50. Voorhees AP, Hua Y, Brazile BL, et al. So-called lamina cribrosa defects may mitigate IOP-induced neural tissue insult. *Invest Ophthalmol Vis Sci*. 2020;61:15.
51. Sigal IA, Flanagan JG, Ethier CR. Factors influencing optic nerve head biomechanics. *Invest Ophthalmol Vis Sci*. 2005;46:4189–4199.
52. Sigal IA, Flanagan JG, Tertinegg I, Ethier CR. Modeling individual-specific human optic nerve head biomechanics. Part I: IOP-induced deformations and influence of geometry. *Biomech Model Mechanobiol*. 2009;8:85–98.
53. Roberts MD, Liang Y, Sigal IA, et al. Correlation between local stress and strain and lamina cribrosa connective tissue volume fraction in normal monkey eyes. *Invest Ophthalmol Vis Sci*. 2010;51:295–307.
54. Hua Y, Voorhees AP, Jan NJ, et al. Role of radially aligned scleral collagen fibers in optic nerve head biomechanics. *Exp Eye Res*. 2020;199:108188.
55. Zhang L, Albon J, Jones H, et al. Collagen microstructural factors influencing optic nerve head biomechanics. *Invest Ophthalmol Vis Sci*. 2015;56:2031–2042.
56. Hua Y, Voorhees AP, Sigal IA. Cerebrospinal fluid pressure: revisiting factors influencing optic nerve head biomechanics. *Invest Ophthalmol Vis Sci*. 2018;59:154–165.
57. Lisboa R, Leite MT, Zangwill LM, Tafreshi A, Weinreb RN, Medeiros FA. Diagnosing preperimetric glaucoma with spectral domain optical coherence tomography. *Ophthalmology*. 2012;119:2261–2269.
58. Lee EJ, Kim T-W, Kim H, Lee SH, Girard MJ, Mari JM. Comparison between lamina cribrosa depth and curvature as a predictor of progressive retinal nerve fiber layer thinning in primary open-angle glaucoma. *Ophthalmol Glaucoma*. 2018;1:44–51.
59. Ren R, Yang H, Gardiner SK, et al. Anterior lamina cribrosa surface depth, age, and visual field sensitivity in the Portland Progression Project. *Invest Ophthalmol Vis Sci*. 2014;55:1531–1539.
60. Sredar N, Ivers KM, Queener HM, Zouridakis G, Porter J. 3D modeling to characterize lamina cribrosa surface and pore geometries using in vivo images from normal and glaucomatous eyes. *Biomed Opt Express*. 2013;4:1153–1165.
61. Darwich R, Jarrar F, Syed M, Sharpe GP, Chauhan BC. Analysis of deep optic nerve head structures with spectral domain and swept-source optical coherence tomography. *Br J Ophthalmol*. Published online July 2023, doi:10.1136/bjo-2023-323222.
62. Tran H, Wallace J, Voorhees AP, et al. Lamina cribrosa shape is different between humans and monkeys at baseline IOP and is changed differently with IOP elevations. *Invest Ophthalmol Vis Sci*. 2017;58:3157.
63. Rasmussen CA, Kaufman PL. Primate glaucoma models. *J Glaucoma*. 2005;14:311–314.
64. Burgoyne CF. The non-human primate experimental glaucoma model. *Exp Eye Res*. 2015;141:57–73.
65. Tran H, Jan N-J, Hu D, et al. Formalin fixation and cryosectioning cause only minimal changes in shape or size of ocular tissues. *Sci Rep*. 2017;7:12065.
66. Brown DJ, Morishige N, Neekhra A, Minckler DS, Jester JV. Application of second harmonic imaging microscopy to assess structural changes in optic nerve head structure ex vivo. *J Biomed Opt*. 2007;12:024029.
67. Jones HJ, Girard MJ, White N, et al. Quantitative analysis of three-dimensional fibrillar collagen microstructure within the normal, aged and glaucomatous human optic nerve head. *J R Soc Interface*. 2015;12(106):20150066.
68. Pijanka JK, Markov PP, Midgett D, et al. Quantification of collagen fiber structure using second harmonic generation imaging and two-dimensional discrete Fourier transform analysis: application to the human optic nerve head. *J Biophotonics*. 2019;12:e201800376.
69. Vohnsen B, Artal P. Second-harmonic microscopy of ex vivo porcine corneas. *J Microsc*. 2008;232:158–163.
70. Raoux C, Chessel A, Mahou P, Latour G, Schanne-Klein MC. Unveiling the lamellar structure of the human cornea over its full thickness using polarization-resolved SHG microscopy. *Light Sci Appl*. 2023;12:190.
71. Sanfilippo PG, Cardini A, Sigal IA, et al. A geometric morphometric assessment of the optic cup in glaucoma. *Exp Eye Res*. 2010;91:405–414.
72. Sanfilippo PG, Cardini A, Hewitt AW, Crowston JG, Mackey DA. Optic disc morphology–rethinking shape. *Prog Retin Eye Res*. 2009;28:227–248.
73. Pierce SE, Angielczyk KD, Rayfield EJ. Patterns of morphospace occupation and mechanical performance in extant crocodilian skulls: a combined geometric morphometric and finite element modeling approach. *J Morphol*. 2008;269:840–864.
74. Stayton CT. Application of thin-plate spline transformations to finite element models, or, how to turn a bog turtle into a spotted turtle to analyze both. *Evolution*. 2009;63:1348–1355.
75. Jan N-J, Sigal IA. Collagen fiber recruitment: a microstructural basis for the nonlinear response of the posterior pole of the eye to increases in intraocular pressure. *Acta Biomater*. 2018;72:295–305.
76. Levy NS, Crapps EE. Displacement of optic nerve head in response to short-term intraocular pressure eleva-

Investigative Ophthalmology & Visual Science

tion in human eyes. *Arch Ophthalmol*. 1984;102:782–786.

77. Girard MJ, Beotra MR, Chin KS, et al. In vivo 3-dimensional strain mapping of the optic nerve head following intraocular pressure lowering by trabeculectomy. *Ophthalmology*. 2016;123:1190–1200.
78. Sigal IA, Grimm JL. A few good responses: which mechanical effects of IOP on the ONH to study? *Invest Ophthalmol Vis Sci*. 2012;53:4270–4278.
79. Sanfilippo PG, Grimm JL, Flanagan JG, Lathrop KL, Sigal IA. Application of Elliptic Fourier analysis to describe the lamina cribrosa shape with age and intraocular pressure. *Exp Eye Res*. 2014;128:1–7.
80. Reynaud J, Lockwood H, Gardiner SK, Williams G, Yang H, Burgoyne CF. Lamina cribrosa microarchitecture in monkey early experimental glaucoma: global change. *Invest Ophthalmol Vis Sci*. 2016;57:3451–3469.

Investigative Ophthalmology & Visual Science